Received: 1 March 2022 | Accepted: 27 July 2022 | Published online: 1 November 2022

DOI: 10.1002/saj2.20473

Soil Science Society of America Journal

SOIL MINERALOGY

Base cations release in soils along the 127-year Hailuogou glacial retreat chronosequence

Nuria Basdediós[1] | **Yanhong Wu**[2] | **Wolfgang Wilcke**[1]

[1]Karlsruhe Institute of Technology (KIT), Institute of Geography and Geoecology, Reinhard-Baumeister-Platz 1, 76131, Karlsruhe, Germany

[2]Key Laboratory of Mountain Surface Processes and Ecological Regulation, Institute of Mountain Hazards and Environment, Chinese Academy of Sciences, Chengdu 610041, China

Correspondence
Wolfgang Wilcke, Institute of Geography and Geoecology, Karlsruhe Institute of Technology (KIT), Reinhard-Baumeister-Platz 1, 76131 Karlsruhe, Germany.
Email: wolfgang.wilcke@kit.edu

Assigned to Associate Editor Caitlin Hodges.

Funding information
National Natural Science Foundation of China, Grant/Award Number: 42271064; Deutsche Forschungsgemeinschaft, Grant/Award Number: WI 1601/25-1

Abstract

At the Hailuogou glacial retreat chronosequence, a mature forest has surprisingly fast developed in ~120 yr, although the glacial debris is dominated by nutrient-poor granite with a small contribution of carbonate minerals. In previous work, we hypothesized that the fast vegetation development is synchronized with initial fast carbonate weathering followed by slow silicate weathering. To test this hypothesis, we (a) characterized the composition of the glacial debris to elucidate the sources of base cations and (b) determined the base cation release kinetics from topsoils (0–10 cm) along the chronosequence with a weathering experiment at a constant pH value (pH_{stat}). Besides granitic rocks, the glacial debris contained some meta-sedimentary and meta-volcanic calc-silicate rocks, amphibolite, mica schist, and quartzite. Although the total Ca concentration of the glacial debris was only about double that of Mg, K, and Na, during the 1st day of the pH_{stat} experiment, the released mass of Ca was >10 times higher than that of Mg and K, and even about 100 times higher than that of Na. The size of the fast-reacting Ca-carbonate pool decreased quickly in the first approximately 40 yr, after which a slow-reacting Ca-silicate pool matched the fast-reacting pool with a size of 1.9 ± 0.6 g kg^{-1} Ca. In contrast, for Mg, K, and Na the slow-reacting pool dominated from the beginning, suggesting that these elements mainly originated from silicate weathering. Our findings support the view that the well-synchronized interplay between carbonate and silicate weathering facilitated the fast vegetation succession.

1 | INTRODUCTION

Chronosequences and associated space-for-time substitutions have been widely used to study the soil development and plant succession across multiple time scales and many landscapes (Bockheim, 1980; Huggett, 1998; Walker et al., 2010). The parent material determines the original element concentrations of the evolved soils and directly influences the balance between nutrient availability, loss, and retention (Anderson, 1988; Augusto et al., 2017; Eimil-Fraga et al., 2014; Jesse Hahm et al., 2014). The weathering of parent materials releases nutrients into the soil solution at variable rates, depending on mineral properties, climatic conditions, topographic position, time, and biota (Harley & Gilkes, 2000; Jenny, 1941; Wilson, 2004). Except for N which usually enters the soil via microbial fixation from the atmosphere, mineral

Abbreviations: DI, deionized water; ECEC, effective cation-exchange capacity; LOI, loss on ignition; MS, meta-sedimentary rock; MV, meta-volcanic rock; PE, polyethylene.

weathering releases all macronutrients (i.e., K, Ca, Mg, P, and S) as well as trace elements which are necessary for plant growth (Barker et al., 1997; Marschner, 2012; Tripler et al., 2006; Vitousek & Sanford, 1986; P. White & Broadley, 2003).

In the subtropical high mountainous Gongga region, located at the southeastern edge of the Tibetan Plateau, the decrease in the mean annual precipitation and increase in the mean annual temperature in the past two decades (Wu et al., 2013) accelerated the retreat of the Hailuogou glacier, one of the largest glaciers at the foot of the Gongga Mountain (Zhou et al., 2013), which started in the late 19th century (Li et al., 2010). The successive ecosystem development created a natural soil and vegetation chronosequence, which has not been disturbed much by human activities. The fast vegetation succession is surprising, because the Gongga Mountain and the derived glacial debris is mainly composed of granite (Searle et al., 2016), a nutrient-poor substrate, particularly with respect to Ca and Mg (Schmitt et al., 2012). However, the Hailuogou glacial debris also contains carbonates originating from meta-sedimentary rocks (Roger et al., 1995; Searle et al., 2016), which are leached out of the topsoil in 47 yr after glacial retreat (Basdediós et al., 2022).

The major rock-forming mineral groups in the Earth's crust are quartz, feldspars (i.e., K-feldspar and plagioclase) and ferromagnesian minerals (e.g., biotite and hornblende). Quartz contains low concentrations of plant nutrients and is little weatherable (Barker et al., 1997). Feldspars persist in strongly weathered soils in which other primary minerals have been altered to secondary minerals, providing a slow release of K and Ca (Allen & Hajek, 1989). In contrast, ferromagnesian minerals are considered to be relatively unstable among the common rock minerals and can release large quantities of Mg and K (Allen & Hajek, 1989). Minerals with higher solubility in water than silicates, such as carbonates, are the most easily weathered (Smith & Huyck, 1999). Fast initial weathering of $CaCO_3$ and the subsequent release of available nutrients may contribute to the development of primary vegetation successions, especially in glacial environments, because chemical weathering is strongly influenced by carbonate minerals even if they are present in only small amounts (~1%) in the parent material (Blum et al., 1998).

The presence of carbonate minerals buffers the pH near neutral values and usually releases Ca and if dolomite or magnesite are present also Mg at high rates through weathering (Mavris et al., 2010; Zamanian et al., 2016). The soil pH influences many biogeochemical processes which drive vegetation succession, such as microbial turnover of organic matter and related N release (Andersson & Nilsson, 2001), P availability (Hinsinger, 2001; Sohrt et al., 2017), and the release of nutrient cations by mineral weathering (Chadwick & Chorover, 2001). Weathering of carbonate and silicate minerals can be described as an acid-base reaction, with the difference that carbonate minerals dissolve completely whereas silicate weathering usually results in the formation of secondary clay minerals outside the inner (per-)humid tropics with their desilicating weathering regime. A mix of mineral constituents in the parent material, for example, carbonates and easily weatherable silicates, might release a wide variety of nutrients through weathering that become easily available for plant uptake. Once a soil organic layer is established, it can store and supply a large quantity of the nutrients required by the vegetation (Basdediós et al., 2022; Jobbágy & Jackson, 2004; Lilienfein et al., 2001; Wilcke et al., 2002). Because at the beginning of the vegetation succession on glacial debris the soil is usually free of organic matter, mineral weathering together with the nutrient input by atmospheric deposition drives the supply of all macronutrients but N, which is acquired by microbial N_2 fixation from the atmosphere except in bituminous sediments and metamorphites (Houlton et al., 2018). Therefore, weathering rates play a crucial role in enabling plant growth. Likewise, plants can influence weathering rates compared with the rates when plants are absent (Berner et al., 2004). Plants cause physical weathering by root growth and influence chemical weathering of minerals to mobilize nutrients from the soil, partly assisted by mycorrhizal fungi with which plant roots are associated. Roots can also excrete organic acids and chelates into the rhizosphere, which help plants to access specific nutrients or to form nontoxic complexes in soils (Drever & Stillings, 1997; Meyer et al., 2009). In a previous study at the Hailuogou glacial retreat chronosequence, Basdediós et al. (2022) suggested that the synchronization of weathering rates with vegetation development facilitated the fast succession. They hypothesized that in the early phase of the ecosystem succession, weathering of carbonates and easily weatherable silicates released high amounts of Ca and to a lesser degree Mg. After carbonates were dissolved, the onset of slower silicate weathering concurring with the shift from deciduous to coniferous forest slowed the nutrient cycle. While the total stocks of Ca and Mg decreased along the

Core Ideas

- Calcite occurred in the mainly granitic substrate of the Hailuogou chronosequence.
- The calcite originated from meta-sedimentary and meta-volcanic rocks in the glacial debris.
- Carbonate weathering determined the rapid initial Ca but not Mg release.
- The main sources of weathered Mg, K, and Na were silicate minerals.
- Base cation release kinetics followed the order, Ca>>Mg>K>>Na.

chronosequence in response to the loss of carbonates and easily weatherable silicates within a few decades, those of K and Na were unrelated with ecosystem age. To explain the lack of a relationship between ecosystem age and K and Na stocks, Basdediós et al. (2022) suggested that K and Na were constantly released from silicate mineral pools at low rates which were taken up by the organisms of the ecosystem with little losses.

Batch and column techniques are used to examine buffer capacities and reaction kinetics of rocks and soils (Alt et al., 2013; Hacker et al., 2017; Selim & Amacher, 1997). Frequently, the analyzed mineral material is exposed to a constant elevated H^+ pressure in so-called pH_{stat} experiments, which can be realized in automatic titroprocessors or as a batch experiment with ion exchangers. In automatic titroprocessors, the proton activity in the reaction solution is kept constant at a higher level than soil equilibrium pH by measuring pH continuously and replacing buffered protons by the addition of mineral acid (Süsser, 1987; van de Sand & Fischer, 1994). In experiments with tritroprocessors, the released ions accumulate in the solution with the risk that secondary mineral precipitation occurs if dissolution constants are surpassed. Titroprocessor experiments therefore mimic conditions with a stagnant solution phase. In the pH_{stat} method of Kaupenjohann and Wilcke (1995) ions released into solution during H^+ buffering are removed from the system with the help of ion exchange resins and therefore do not affect further reactions. Ion exchange resin approaches mimic conditions in which water percolates through the soil and removes weathering products (Alt et al., 2013; Hacker et al., 2017; Schwarz et al., 1999). Süsser (1987) described buffer reactions in soils during pH_{stat} experiments as the sum of two independent reactions both following first order kinetics. This allows to distinguish a fast- and a slow-reacting mineral pool and release rate constants associated with these pools.

Our overall objective was to (a) identify the origin of the carbonate minerals in the granite-dominates glacial debris of the Hailuogou glacier and test the hypotheses that (b) $CaCO_3$ determines initial Ca release and contributes, to a minor degree, to that of Mg; (c) the weathering release rates of Ca and Mg decrease with increasing soil age, because of the fast loss of initially present carbonates and easily weatherable silicate minerals as reflected by strongly decreasing fast-reacting Ca and Mg pools. Once the carbonates are gone, the slower silicate weathering takes over and releases Ca and Mg at lower rates than initially, which is synchronized with the ecosystem development from deciduous to coniferous forest. (d) Potassium and Na are only weathered from silicate minerals such as mica during the whole ecosystem development and thus show constant release rates and slightly decreasing pool sizes.

2 | MATERIALS AND METHODS

2.1 | Study area

The Gongga Mountain (summit: 7,556 m asl, Figure 1) is formed from the Gongga batholith, which extends for more than 100 km in the transition zone of the Sichuan Basin and the Tibetan Plateau, southwest China. The massif is mainly composed of a granitoid complex (i.e., granite and granodiorite) intruded into the Palaeozoic–Triassic meta-sediments and meta-volcanic rocks of the Songpan-Ganze terrane (Roger et al., 1995; Searle et al., 2016). Located on the eastern slope of the Gongga Mountain, the Hailuogou Glacier has markedly retreated since the late 19th century (Li et al., 2010), developing a 2-km long and 50–200-m wide chronosequence, which spans an elevational range from 2,800 to 2,950 m asl. The short time of pedogenesis (<130 yr) formed soils without B horizon classified from youngest to oldest as Leptic Calcaric to Folic Dystric Regosols (IUSS Working Group WRB, 2014). The parent material of soil formation is moraine and consists mainly of a mixture of silicates (87%), including plagioclase (28.5%), quartz (24.5%), biotite (12%), hornblende (12%), and K-feldspar (10%), carbonates (<10%), and a minor contribution of apatite (<2.1%) (Yang et al., 2015; Zhou et al., 2016). The mean annual temperature and precipitation are 4.2 ˚C and 1,947 mm, respectively. Rain falls mainly during the summer growing season (May–September) (Wu et al., 2013).

Our study included seven sites, deglaciated between 0 (Site 1: 2,982 m asl) and 127 yr ago (Site 7: 2,855 m asl; Figure 1), previously described by Zhou et al. (2013). A primary vegetation succession has developed along the chronosequence, from pioneer shrubs (i.e., *Hippophae rhamnoides* L.; Site 3: 37 yr), over half mature broad-leaved tree forests dominated by poplar (*Populus purdomii* Rehder; Site 4: 47 yr), to a full conifer forest dominated by Faber's fir [*Abies fabri* (Mast.) Craib; Sites 5 and 6: 59 and 87 yr, respectively] and Sargent spruce [*Picea brachytyla* (Franch.) E. Pritz.; Site 7: 127 yr]. With increasing time, the soils have developed A and O horizons of increasing thickness. The intense carbonate weathering in the early stage of the chronosequence and the rapid establishment of the vegetation decreased soil pH from 8.0 to 5.8 in only 47 yr (Basdediós et al., 2022).

2.2 | Field sampling

At all seven study sites, we collected samples of the A and C horizons and from the 0-to-10-cm topsoil layer, which included the uppermost part of the C horizons because the morphologically recognizable A horizons were only

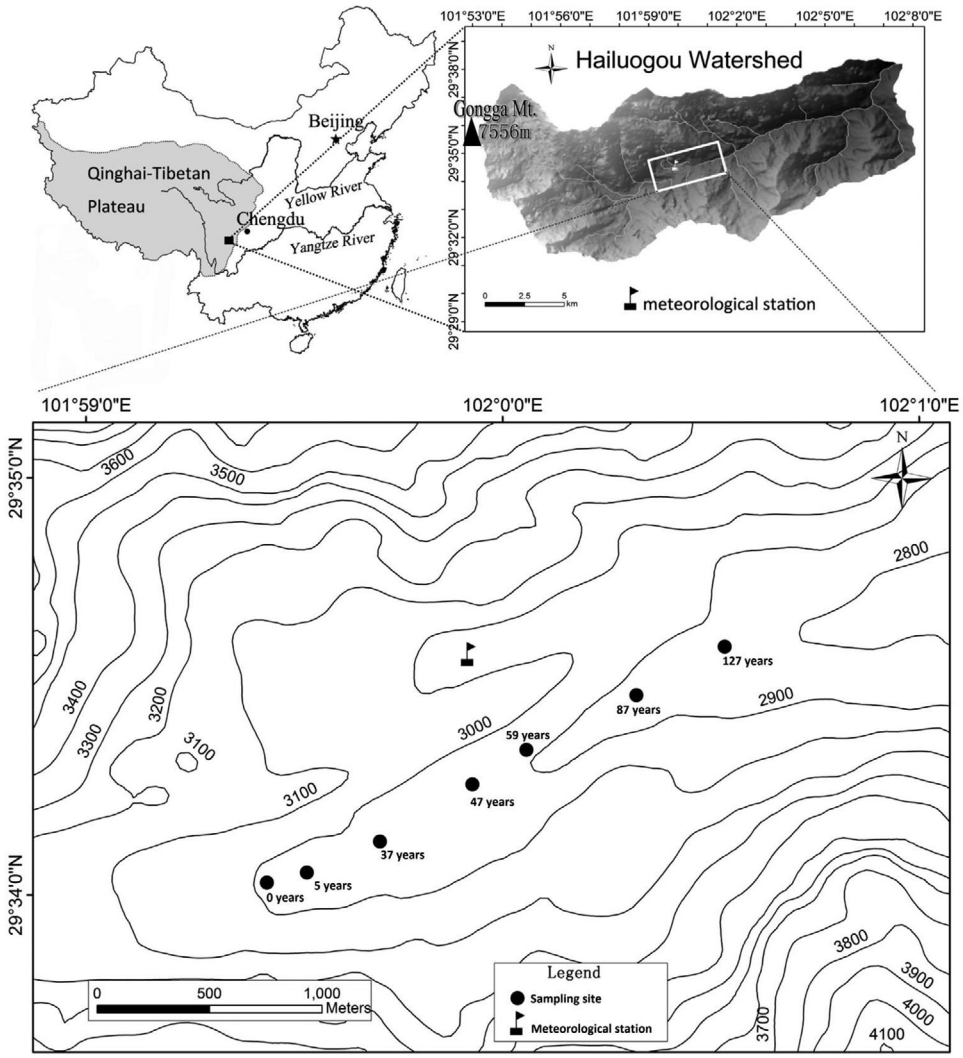

FIGURE 1 Location of the Hailuogou chronosequence and study sites (Basdediós et al., 2022)

0.5–6.5-cm thick or even absent at Site 1 in August 2017 (Figure 1; Table 1). Each ecosystem succession stage was sampled in triplicate. The distance between the sampled soil profiles was at least 20 m, except at Sites 1 and 2, where the distance was reduced to 10 m because of the narrower valley in the proximity of the glacier. Mineral soil samples were air-dried to constant weight and sieved to two different fractions: fine earth (<2 mm) and stones (>2 mm). Plant residues were removed manually. At Site 1 (0 yr), we additionally collected 16 different rock samples from the surface which we considered as representative of the composition of the glacial debris forming the substrate for soil development.

2.3 | Optical and chemical analyses

To determine the type of the collected rocks, photomicrographs of thin sections (30-μm thick) were taken with an Axiocam 105 attached to a Zeiss Axiolab optical microscope (1.5×; Carl Zeiss AG). To collect unweathered rock material, we removed the outer shell of each rock sample by cutting with an automated core slabbing saw. Aliquots of the soil samples were ground using a Retsch MM 400 ball mill (Retsch GmbH). The stone fraction of the soils (>2 mm) and the rock samples were ground in an agate grinding set using a vibratory disk mill (Siebtechnik GmbH).

Total element concentrations in fine earth (<2 mm), the stone fraction (>2 mm), and rocks from the glacial debris, were determined after total digestion with concentrated HNO_3/HF/H_2O_2 (4:1.5:1, v/v) in a microwave oven (MARS6Xpress, CEM) by measurement with an inductively coupled plasma optical-emission spectrometer (ICP-OES, 5100 VDV, Agilent). Accuracy was assessed by the analysis of a certified reference material (BCR-2, Basalt). Average recoveries ± standard deviations were 100 ± 10% for all certified elements.

Soil pH, effective cation-exchange capacity (ECEC), concentrations of exchangeable Ca, Mg, K, and Na, and Ca

TABLE 1 Mean loss on ignition (LOI) and element concentrations with standard errors in parentheses ($n = 3$) of the stone fraction (>2 mm) in the soil profiles along the Hailuogou chronosequence

Site age	Soil horizon	LOI	Inorganic C	S	Ca	Mg	K	Na
yr		%	g kg^{-1}					
5	A	4.38 (1.5)	7.4 (1.0)	0.7 (0.2)	74.5 (4.2)	32.1 (1.2)	36.1 (3.0)	26.1 (1.3)
37	A	0.51 (0.0)	7.3 (0.8)	0.3 (0.2)	70.2 (9.6)	36.3 (5.1)	36.5 (3.4)	24.3 (2.2)
47	A	0.69 (0.1)	2.0 (0.7)	0.1 (0.0)	65.7 (2.2)	31.2 (0.6)	49.2 (2.9)	36.8 (4.5)
59	A	1.27 (0.3)	2.6 (0.7)	0.3 (0.1)	57.1 (5.5)	30.4 (4.1)	40.4 (4.0)	26.9 (3.3)
87	A	1.68 (0.8)	1.5 (0.2)	0.2 (0.1)	45.3 (1.3)	20.5 (2.2)	28.4 (1.9)	21.5 (0.9)
127	A	5.59 (4.5)	2.0 (0.3)	0.3 (0.1)	42.9 (4.7)	19.2 (2.3)	28.9 (0.6)	19.2 (0.9)
5	C	0.20 (0.0)	9.7 (0.2)	0.7 (0.3)	87.4 (2.4)	32.2 (0.5)	37.6 (1.1)	25.3 (2.4)
37	C	0.45 (0.1)	10.2 (3.7)	0.3 (0.1)	60.3 (10.0)	21.8 (4.0)	21.9 (1.6)	14.2 (1.7)
47	C	0.27 (0.1)	1.6 (0.7)	0.1 (0.0)	53.6 (8.1)	26.2 (1.8)	46.6 (3.5)	30.6 (2.4)
59	C	0.57 (0.0)	3.4 (1.1)	0.2 (0.1)	57.7 (6.7)	27.7 (3.0)	39.9 (3.6)	26.4 (3.0)
87	C	0.73 (0.2)	2.4 (0.6)	0.2 (0.1)	35.3 (1.5)	17.0 (0.9)	25.2 (1.9)	17.4 (1.5)
127	C	0.37 (0.1)	1.8 (0.7)	0.3 (0.2)	46.2 (2.7)	21.2 (1.0)	35.5 (1.2)	23.6 (1.3)
0	C1	1.58 (0.3)	6.7 (0.8)	0.3 (0.1)	79.7 (11.5)	31.4 (2.9)	(34.1 (3.0)	28.5 (1.7)
0	C2	0.41 (0.1)	9.5 (2.8)	0.5 (0.3)	88.9 (6.0)	31.8 (3.0)	35.2 (2.3)	25.3 (0.7)

carbonate concentrations were taken from Basdediós et al. (2022). The inorganic C (i.e., after muffling the samples at 550 ˚C to remove organic matter) and total S concentrations of the stone fraction were determined by combustion in a CNS Elemental Analyzer (EuroEA, HEKAtech GmbH). The inorganic C concentrations and $\delta^{13}C$ values in the rocks were determined with an Elemental Analyzer – Isotope Ratio Mass Spectrometer (Flash 2000 HT Plus-Delta V Advantage, ThermoFisher Scientific) after muffling the samples at 550 ˚C. Loss on ignition (LOI) was determined by weighing before and after muffling the samples at 550 ˚C.

To determine the release kinetics of the base cations (i.e., Ca, Mg, K, and Na) we followed the method of Schwarz et al. (1999) and included modifications of Alt et al. (2013) to handle the carbonates. We inserted 2 g of a mixed ion-exchange resin (Amberlite MB-20, Rohm and Haas) into 3 cm-wide 4 cm-long homemade polyethylene (PE) bags, which were permeable to fluids (mesh width 100 µm). Before starting the experiment, the resin was saturated with HNO_3 and rinsed with deionized water (DI, >18 MΩ cm^{-1}) to remove free acid. We added 100 ml of DI water to 1 g of fine earth in a 125-ml PE bottle. The soil–water suspension was shaken during 1 h and the initial pH was measured. The resin bag and 1 ml of $Ba(NO_3)_2$ of varying concentrations were added at the same time to the soil–water suspension in equilibrium to start the experiment. We supplied as many Ba equivalents as were theoretically necessary to lower the pH to 3.0 by releasing exchanged H^+ from the resin. The Ba equivalents were calculated as the H^+ concentration in the solution at pH 3.0 minus that in the equilibrium soil suspension, assuming that each mol of Ba^{2+} releases 2 mol of H^+. The bottles were shaken during 10 min, 30 min, 1 h, 2 h, 4 h, 12 h, 24 h, 48 h, 96 h, and 168 h, respectively, to determine the element release over time. Therefore, 10 PE bottles were prepared per soil sample. At each site age, we analyzed three independent soil samples collected from the uppermost 10 cm of the soils. In total, 7 sites × 3 replicates × 10 aliquots for the different shaking times = 210 samples were processed. After the extraction time had passed, the resin bags were removed and the pH of the soil suspension was immediately measured in an aliquot that was afterwards discarded because of the release of K by the glass electrode. After rinsing the resin bags thoroughly with DI water, the ions adsorbed to the resin were extracted in three steps with 30 ml of 2 M HNO_3 for 10 min in the first and second step and for 30 min in the last one. Exchanged element concentrations were determined by ICP-OES. Preliminary tests of the element recovery from the resins with standard solutions were satisfying for all studied elements (Ca: 101 ± 3%, Mg: 99 ± 1%, K: 106 ± 3%, Na: 99 ± 1%; $n = 3$).

2.4 | Calculations and statistical analyses

The initial number of moles of H^+ that had to be released from the resin to decrease the initial pH (pHi) to 3.0 by exchange with Ba^{2+} ions was calculated with Equation 1.

$$H^+ = \left(10^{-3} - 10^{-pHi}\right)/2 \quad (1)$$

The base cation release kinetics were described by a two-step first-order reaction (Equation 2, Schwarz et al., 1999;

Süsser, 1987).

$$Y(t) = \text{PoolA}\left(1 - e^{-k_a t}\right) + \text{PoolB}\left(1 - e^{-k_b t}\right) \quad (2)$$

where $Y(t)$ represents the element release from soil (mg kg^{-1}) at time t. Pool A and Pool B are the estimates of the two differently reactive pools (slow/fast; mg kg^{-1}) and k_a and k_b are the corresponding rate constants (h^{-1}) of each pool, estimated by a nonlinear regression model using sequential quadratic optimization. We used the coefficient of determination (R^2) as a measure of the fit between our data and the function.

Linear regression and Pearson correlation were used to evaluate the relationships between variables. Significant differences between the fast-reacting pool (Pool A) of each base cation (i.e., Ca, Mg, K, and Na) and its respective exchangeable element concentration extracted with 1 M NH_4NO_3 were tested with independent two-sample t tests at each site. One-way ANOVA and Tukey's HSD post-hoc test were applied to find significant differences in Pool A, Pool B, k_a and k_b among the seven study sites. Normal distribution of residuals was visually inspected. Homoscedasticity was tested with Levene's test. Statistical analyses were conducted with the statistical software R (R Core Team, 2019). Significance was set at $p < .05$.

3 | RESULTS

3.1 | Rock types and source of carbonates

The 16 rocks we collected at Site 1 included four samples of granite, six samples of calc-silicate rocks of which five were meta-sedimentary (MS) and one meta-volcanic (MV), three samples of amphibolite, one sample of mica schist and one sample of quartzite. Our visual impression in the field was that meta-volcanic rocks occurred rarely in the study area, while metasedimentary rocks were more frequent.

We detected inorganic C in all collected rock types (Figure 2). Assuming that all the inorganic C is present as calcite ($CaCO_3$), the studied rocks contained up to 19% of calcite. The sample with the highest calcite concentration was the meta-volcanic rock (MV, Figure 2). The second highest inorganic C concentrations were detected in the more frequent metasedimentary rocks (MS). In these rocks, calcite was present together with quartz and amphibole (Figure 3a), epidote (Figure 3b), biotite (Figure 3c), and traces of zoisite (Figure 3d). Optical microscopy images revealed that the calcite occurred mainly in the pores of the rocks, as interstitial calcite between the grains (Figure 3e). The meta-volcanic rock was characterized by layering mainly consisting of calcite, plagioclase, amphibole, feldspar, and traces of quartz (Figure 3f).

Total metal concentrations of the rocks varied widely (Figure 2). Calcium concentrations correlated significantly with the inorganic C concentrations in the calc-silicate rocks and granites ($r = .88$, $p < .001$, $n = 10$). However, this was not the case in amphibolite, mica-schist, or quartzite. The total Mg, K, and Na concentration in rocks did not correlate with the inorganic C concentrations. The $\delta^{13}C$ values ranged from −2.43 to −10.4‰ in all rocks except for amphibolite and mica schist, which were lower (–11.5 to −22.5‰). The rapid carbonate depletion from the parent material was reflected by the fast decrease in inorganic C concentrations in the stone fraction along the chronosequence, which fell by one order of magnitude during the first 47 yr (Table 1).

3.2 | Base cation release kinetics

From Site 1 to Site 3 (soils containing carbonates), the target pH of 3.0 was reached in 4–12 h after starting the experiment, while from Site 4 to Site 7, the target pH was reached in 30 min to 1 h. At Sites 1 (0 yr) and 2 (5 yr), the release kinetics of Ca were converged to a one-pool kinetic equation instead of to a two-pool kinetic equation (Pool B = 0 or $k_a = k_b$). The goodness of the fit (R^2 values) ranged from .89 to .99, .97 to .99, .96 to .99 and .96 to .99 for Ca, Mg, K, and Na, respectively (Figure 4).

The size of the fast-reacting pool (Pool A) of Ca dropped substantially along the chronosequence (Figure 5a) and correlated significantly positively with the $CaCO_3$ and exchangeable and total Ca concentrations (Table 2). Pool A of Mg, K, and Na did not change with site age and was generally smaller than their corresponding slow-reacting Pool B (Figure 5b–d). Pools A of Mg and K were significantly and marginally significantly ($p < .1$) correlated with the exchangeable Mg and K concentrations in soil, respectively (Table 2). Pool B of K correlated positively with the exchangeable K concentrations (Table 2). Pool B of Na increased significantly with decreasing $CaCO_3$ concentrations.

The modeled release rate constant associated with the fast-reacting Pool A, k_a, did not significantly change with site age for any of the studied elements and varied from 0.3 to 0.7, 1.7 to 8.2, 0.4 to 0.8, and 0.1 to 39 h^{-1} for Ca, Mg, K, and Na, respectively. Similarly, the modeled release rate constant associated with the slow-reacting Pool B, k_b, of Ca, Mg, and Na was not correlated with site age, and varied from 0.02 to 0.04, 0.01 to 0.02 and 0.01 to 0.03 h^{-1}, respectively. Only k_b of K decreased significantly with site age, from 0.08 (Site 1, 0 yr) to 0.02 h^{-1} (Site 7, 127 yr). The k_a values of Ca correlated significantly negatively with the total Ca concentrations, while the k_a values of Na correlated significantly negatively with the $CaCO_3$ concentrations. The k_b values of Mg and K correlated significantly positively with pH and $CaCO_3$ concentrations (r and p values shown in Table 2).

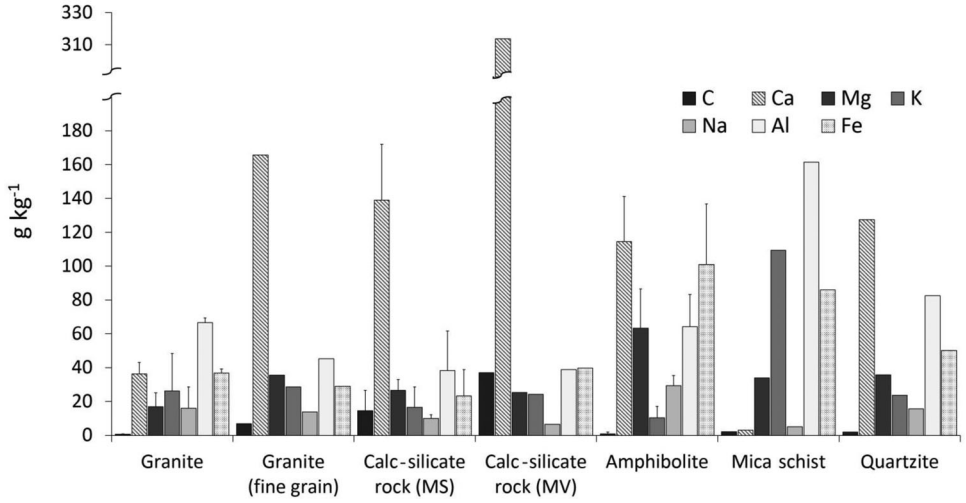

FIGURE 2 Mean concentrations of inorganic C, Ca, Mg, K, Na, Al, and Fe in the sampled rock types of the Hailuogou glacial debris. Error bars indicate the standard deviation of three (granite and amphibolite) or six (calc-silicate rock) replicate samples. Lacking error bars indicate that only one sample was available. MS, metasedimentary rock; MV, metavolcanic rock

TABLE 2 Pearson coefficient (*r*) and *p* values of the correlations of site age, exchangeable element concentrations (exch.) extracted with 1 M NH_4NO_3, $CaCO_3$ concentration, and total element concentrations in the fine earth (soil <2 mm) with Pools A and B and release rate constants k_a and k_b, which were modeled based on the results of a pH_{stat} experiment at pH 3 on the topsoils (0–10 cm) along the Hailuogou chronosequence

	Pool A, mg kg^{-1}		Pool B, mg kg^{-1}		Release rate constants, h^{-1}			
					k_a		k_b	
Properties	***r***	***p***	***r***	***p***	***r***	***p***	***r***	***p***
Ca								
Site age, yr	−.81	<.001	−.50	.06	.42	.06	.23	.40
Exch. Ca, mg kg^{-1}	.93	<.001	.58	<.05	−.38	.09	.29	.29
$CaCO_3$, g kg^{-1}	.99	<.001	.47	.08	−.38	.08	.35	.20
Total Ca soil, g kg^{-1}	.94	<.001	.58	<.05	−.54	< .05	−.06	.84
Mg								
Site age, yr	.17	.47	−.27	.24	−.32	.16	−.40	.07
Exch. Mg, mg kg^{-1}	.54	<.05	−.12	.61	−.38	.09	−.18	.43
$CaCO_3$, g kg^{-1}	.04	.86	−.10	.67	.17	.47	.47	<.05
Total Mg soil, g kg^{-1}	−.18	.45	.28	.22	.13	.56	.30	.19
K								
Site age, yr	−.32	.16	−.40	.07	−.26	.25	−.62	<.05
Exch. K, mg kg^{-1}	.38	.09	.50	<.05	.15	.53	−.02	.93
$CaCO_3$, g kg^{-1}	.07	.76	−.04	.88	.35	.12	.74	<.001
Total K soil, g kg^{-1}	−.21	.37	−.12	.60	.11	.62	−.25	.27
Na								
Site age, yr	.16	.49	.32	.16	.26	.26	−.31	.17
Exch. Na, mg kg^{-1}	−.06	.81	−.21	.36	.36	.11	.18	.44
$CaCO_3$, g kg^{-1}	.00	.99	−.50	<.05	−.48	<.05	.30	.18
Total Na soil, g kg^{-1}	−.13	.57	.40	.07	.28	.21	−.21	.37

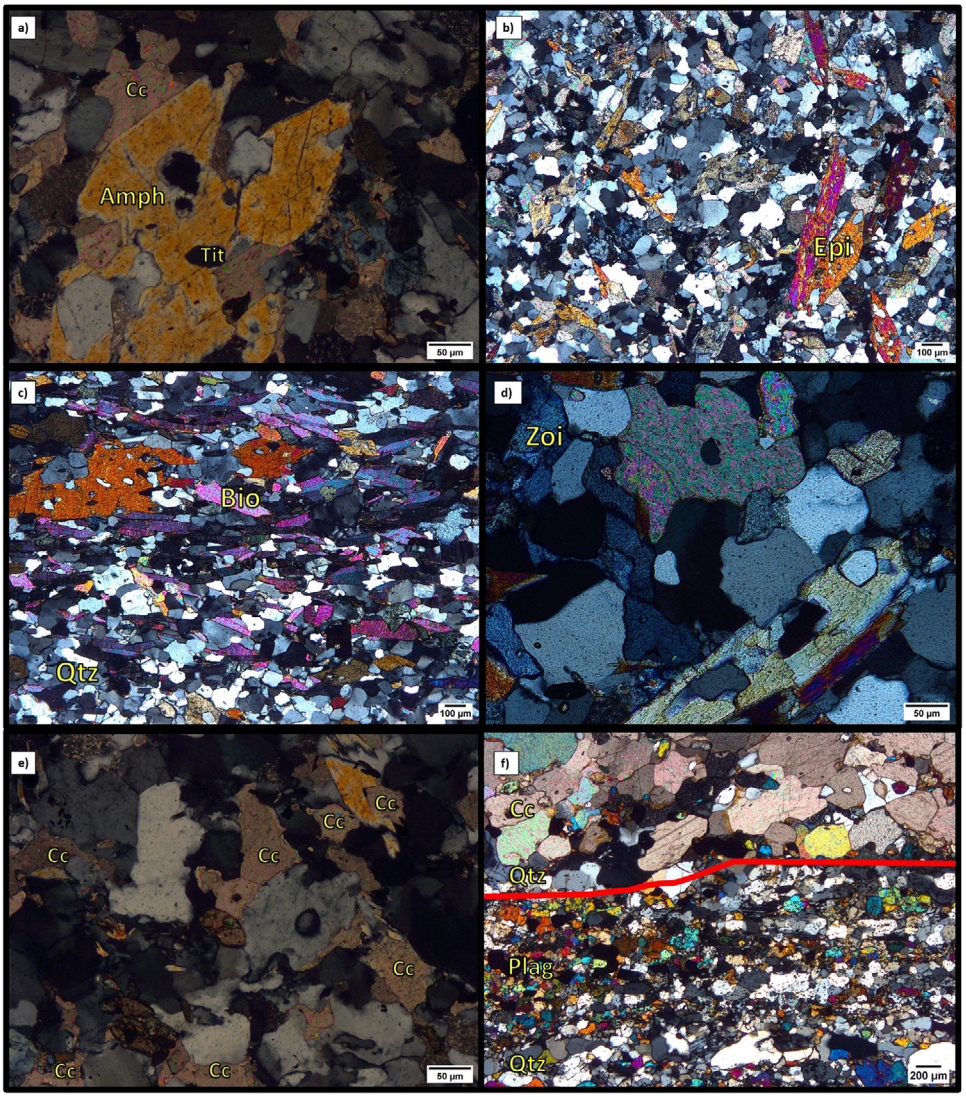

FIGURE 3 Photomicrograph of thin sections of selected rocks collected from the Hailuogou glacial debris. Metasedimentary rocks (a–e) contained (a) calcite (Cc), amphibole (Amph), and titanite (Tit), (b) Epidote (Epi), (c) biotite (Bio), and quartz (Qtz), (d) some zoisite (Zoi), and (e) high amounts of interstitial calcite between the grains. (f) The only meta-volcanic rock collected contained a carbonate layer (Cc), few quartz layers (Qtz) and plagioclase (Plag). The red line in f illustrates the banding/layering by separating the coarser grained upper part from the finer grained lower part of the photomicrograph of the meta-volcanic rock

The size of the Pools A of Ca and Mg generally did not significantly differ from the respective size of the exchangeable element concentrations at most sites (Figure 6a,b). However, at Sites 1 and 2 the Pool A of Mg was significantly larger than the exchangeable Mg concentration and at Site 5 Pools A of Ca and Mg were significantly larger than the respective exchangeable element concentrations. The exchangeable Ca concentration in the carbonate-containing soils (Sites 1–3) could not be determined with the used standard method because of the partial dissolution of calcite in the extract. The size of Pools A of K and Na was significantly larger than the respective exchangeable concentrations at all study sites (Figure 6c,d).

The slow-reacting Pool B of Mg only started to release Mg after 4–12 h and was significantly correlated with the total Mg concentration in the soil ($r = .59$). Pools B of Mg and K correlated significantly with each other ($r = .65$, $p = .001$) but not with those of Ca or Na. At the end of the experiment ($t = 168$ h), the total mass of released Mg strongly correlated with that of Fe ($r = .96$, $p < .001$), Al ($r = .89$, $p < .001$), and K ($r = .84$, $p < .001$). However, there was no correlation between the total mass of released Ca and Na and that of Fe or Al. The released K/Mg ratio 1 h after starting the experiment linearly decreased from 3.1 ± 0.3 (Site 1) to 0.9 ± 0.2 (Site 7, $r = .79$, $p < .005$), while it averaged 0.4 ± 0.1 at the end of the experiment with little variation (Figure 7a). Similarly, the

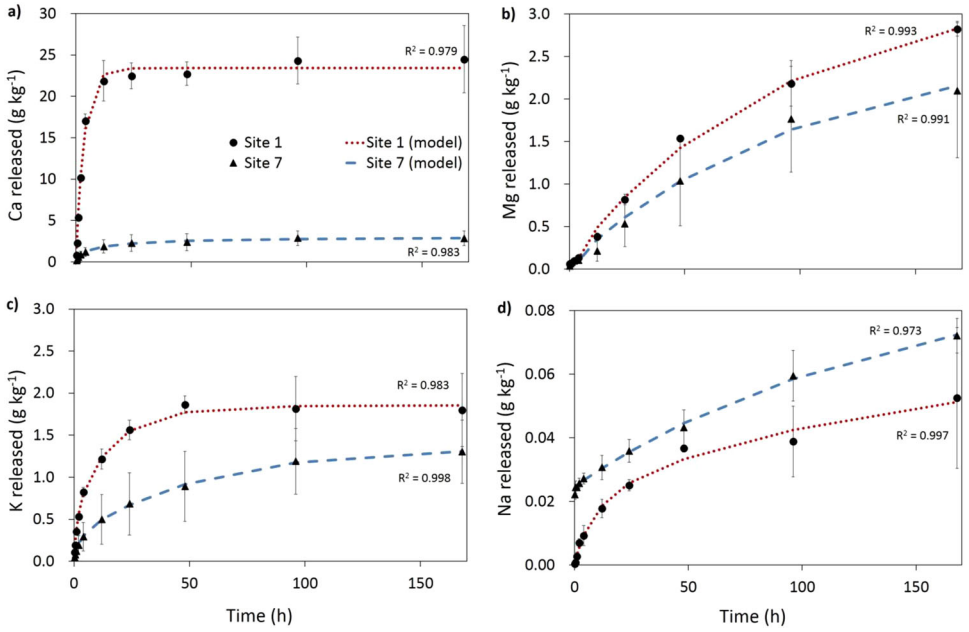

FIGURE 4 Release kinetics of (a) Ca, (b) Mg, (c) K, and (d) Na during a pH_{stat} experiment at pH 3 in topsoils (0–10 cm) from Site 1 (0 yr) to Site 7 (127 yr) of the Hailuogou chronosequence. Error bars represent standard errors ($n = 3$). The dotted and dashed lines illustrate the biexponential fit

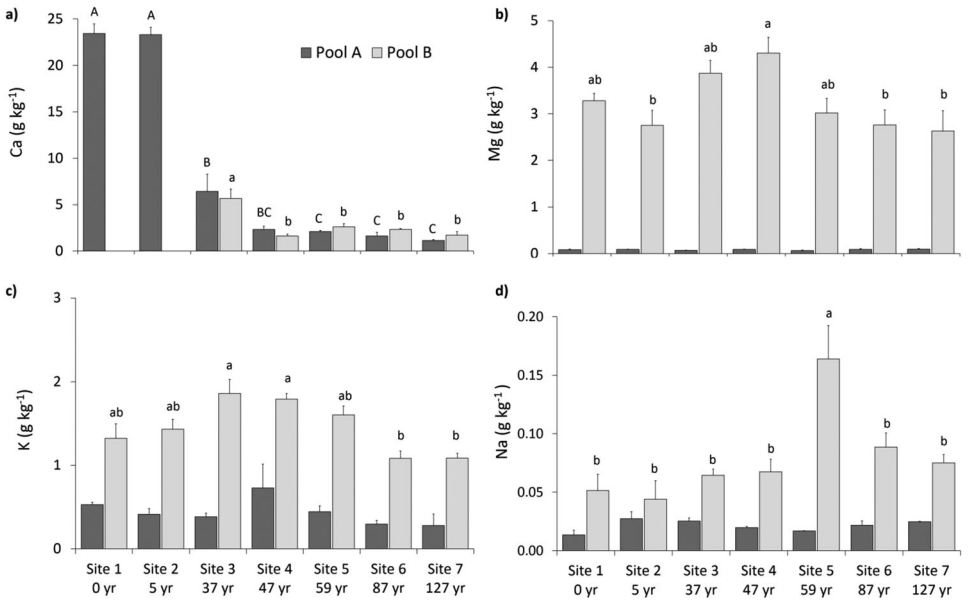

FIGURE 5 Sizes of (a) Ca, (b) Mg, (c) K, and (d) Na Pools A (fast) and B (slow) in topsoils (0–10 cm) calculated with the biexponential function in Equation 2 along the Hailuogou chronosequence. Uppercase and lowercase letters denote significant differences in the sizes of Pools A and B, respectively, among the sites ($p < .05$). Error bars represent standard errors ($n = 3$)

molar K/Mg ratio in aboveground biomass tended to decrease from Site 3 to 7, although the correlation between site age and molar K/Mg ratio was not significant (Figure 7b). The molar K/Mg ratio varied little with site age in the organic layer and the mineral soil (0–10 cm).

4 | DISCUSSION

4.1 | Source of carbonates

The plutonic component of the Hailuogou glacial debris was expected from geological maps showing that the Gongga

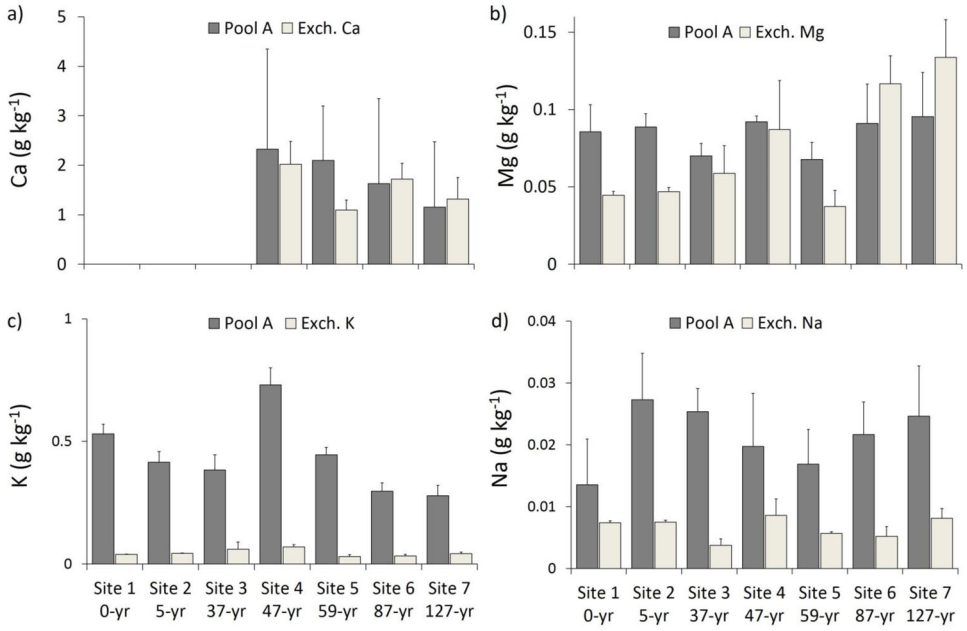

FIGURE 6 Sizes of the fast-reacting Pool A of (a) Ca, (b) Mg, (c) K, and (d) Na and size of the respective exchangeable element pools extracted with 1 M NH_4NO_3 from topsoils (0–10 cm). The exchangeable Ca concentration in the carbonate-containing soils (Sites 1–3) could not be determined with the used standard method because of the partial dissolution of calcite in the extract

Mountain peak is composed of granitic rocks. Paleozoic sedimentary rocks with high-grade metamorphism can be found in the surroundings, ~10 km from the main peak (Roger et al., 1995). Searle et al. (2016) also reported the presence of metasediments at the eastern margin of the Gongga batholith, which also belongs to the source area of the Hailuogou glacial debris.

Our suggestion that the inorganic C detected in all sampled rocks (Figure 2) was mainly calcite (Figure 3) is supported by its $\delta^{13}C$ values, which were similar to those reported for carbonates in metamorphic and igneous rocks of −11.9 to +3.1‰ (Deines & Gold, 1973) and of −16 to +2‰ in calc-silicate rocks (Schwarcz, 1969). However, the amphibolite and mica schist samples which had $\delta^{13}C$ values ≤−16‰, may have contained graphite, for which $\delta^{13}C$ values down to −41‰ are reported (Deines, 1980; Ghent & O'Neil, 1985). This assumption is supported by the finding that no strong reaction was observed after application of diluted HCl to the amphibolite and mica schist samples.

Optical microscopy images revealed that calcite was mainly present in the pores of the metasedimentary rocks as interstitial calcite between the grains (Figure 3e), which is in line with findings of A. White et al. (1999) who reported that calcite can occur as fillings in cracks and microfractures within the silicate matrix. Moreover, in some of our samples the saussuritization process by which primary rock-forming plagioclase is partially transformed into other minerals, such as epidote, zoisite, albite, or calcite could also have occurred. Saussuritization was observed in other mainly granitic proglacial areas such as the Morteratsch glacial retreat area in the Canton of Grisons, Switzerland (Mavris et al., 2010). The Morteratsch glacial retreat area is one of the few locations we know of, where similar to the Hailuogou region, a fast vegetation cover has developed within few decades after glacial retreat. However, the $CaCO_3$ concentration in the Morteratsch glacial debris is with only 0.2 ± 0.3% (Mavris et al., 2010) one order of magnitude lower than at Hailuogou (5.6%) (Zhou et al., 2016).

We even detected low concentrations of carbonates in the abundant coarse-grained granites (3–7 g kg^{-1} $CaCO_3$, Figure 2) and higher ones in the fine-grained granite from the Hailuogou area (57 g kg^{-1} $CaCO_3$, Figure 2). Up to now, the petrogenesis of calcite in granitoid rocks has received little attention. A. White et al. (2005) stated that calcite is universally present in granitoid rocks in a concentration ranging from 0.028 to 18.8 g kg^{-1}, with a mean of 2.52 g kg^{-1}. To explain the ubiquitous presence of accessory calcite in granitoid rocks, A. White et al. (2005) suggested that calcite might be included during late-magmatic growth or subsolidus replacement during magmatic processes. However, specific calcite occurrences can also be related to external inputs, such as from carbonate wall rocks or hydrothermal alteration (A. White et al., 2005). Geothermal mid-temperate springs (T~60 °C) are scattered across the Hailuogou National Forest Park (Qi et al., 2017). Because of the presence of Paleozoic sedimentary rocks in the eastern catchment area of the Hailuogou glacier (Searle et al., 2016) in combination with hydrothermal sources in the surroundings of the study area (Qi et al., 2017),

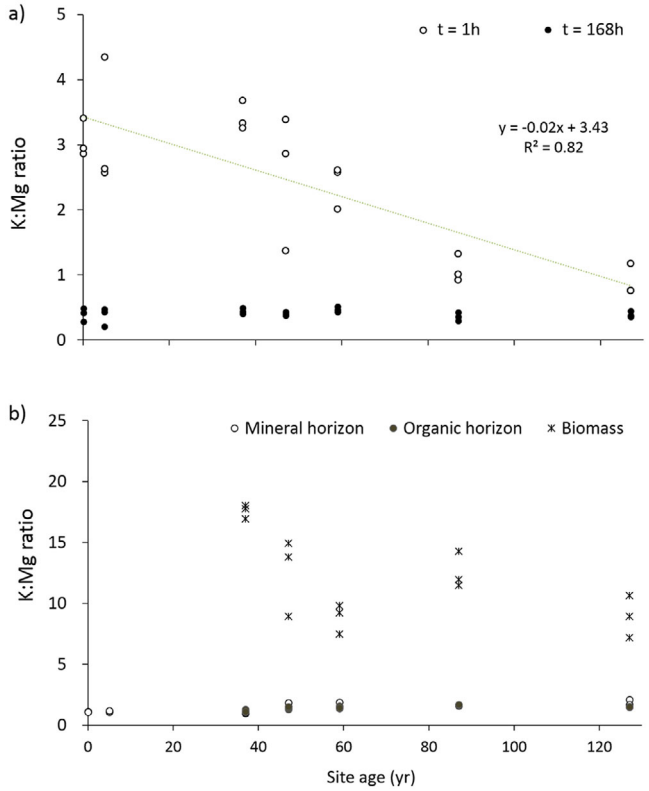

FIGURE 7 (a) Released molar K/Mg ratios 1 and 168 h after starting the pH_{stat} experiment and (b) molar K/Mg ratios in the upper 10 cm of the mineral soil, the organic layer, and the aboveground biomass along the chronosequence. For each site age, we ran three independent batch experiments and collected three independent samples, which are individually shown. The regression line in a was calculated for the means of each site age. Data of b were taken from Basdediós et al. (2022)

we suggest that the detected inorganic C in the granite samples of the Hailuogou chronosequence can be attributed to a mix of magmatic processes and external inputs.

4.2 | Role of carbonates and easily weatherable silicates for the release of Ca and Mg

The release of all studied base cations by acid hydrolysis initially proceeded fast, followed by a slower reaction (Figure 4). Although the total Ca concentration of the parent substrate was only about double that of Mg, K, and Na (Table 1), during the 1st day of the pH_{stat} experiment, a >10 times higher mass of Ca was released than of Mg and K and even approximately 100 times higher mass of Ca than of Na (Figure 4). Rapid element release at the beginning of a pH_{stat} experiment is likely related to cation-exchange reactions and unstable solid phases that are easily dissolved upon acidification, for example, carbonates (Alt et al., 2013; Cappuyns & Swennen, 2008). The fact that along the Hailuogou chronosequence, the size of the fast-reacting Ca pool (Pool A) correlated positively with the carbonate (CO_3^{2-}), exchangeable Ca, and total Ca concentrations in soil, while the fast-reacting Mg pool only correlated with the exchangeable Mg concentrations in soil (Table 2), suggested that the Mg release along the chronosequence was not associated with the weathering of Mg-containing carbonate minerals, such as dolomite or magnesite, but with cation-exchange reactions.

Along the chronosequence, the size of the fast-reacting Ca and Mg pools did not significantly differ from the respective sizes of the exchangeable element pools (Figure 6a,b), except for Mg in the younger soils (Sites 1 and 2), where the Pool A was larger than the exchangeable Mg concentrations (Figure 6b). This may be attributed to the release of Mg from other labile minerals, such as chlorite (Zhou et al., 2016) during the pH_{stat} experiment.

4.3 | Changes of Ca and Mg weathering rates with ecosystem development

The comparison of the release kinetics of the four base cations between Sites 1 and 7 revealed a general slowdown of the weathering for all studied elements, except for Na (Figure 4). However, the difference in the release kinetics between Sites 1 and 7 was particularly pronounced for Ca and comparatively weak and similar for the other three elements. We attribute this to the loss of carbonates within a few decades, from which only Ca was released to a considerable extent.

The release rate constant associated with the fast-reacting Ca pool, k_{a_Ca}, increased with decreasing Ca concentration in soil and marginally significantly with soil age (Table 2). This occurred in line with the rapid weathering of carbonates reported by Basdediós et al. (2022). After carbonates were leached (>47 yr), the size of the fast-reacting Ca pool was comparable to that of the exchangeable Ca pool (Figure 6a). The release rate constant associated with the slow-reacting Pool B of Ca, k_{b_Ca}, did not significantly change with increasing site age, although the size of Pool B tended to decrease (Table 2). This indicated that the slow-reacting Ca pool was weathered at a constant rate along the chronosequence. We suggest that Ca-Al sorosilicates, such as titanite and epidote (Figure 3a,b), contributed to the slow-reacting pool of Ca (Figure 5a).

The release rate constant associated with the fast-reacting Mg pool, k_{a_Mg}, did not significantly change along the chronosequence, while that associated with the slow-reacting Mg pool, k_{b_Mg}, marginally significantly ($p < .1$) decreased with time. Unexpectedly, the slow-reacting Mg pool seemed to only become active 4–12 h after the start of the experiment and not simultaneously with the fast pool as was the case for Ca, K, and Na (Figure 4), which may indicate that

Mg was more strongly bound in soil, for example, by association with highly insoluble soil constituents (Cappuynus & Swennen, 2008). The acid target pH of 3.0 in our pH_{stat} experiment intensified the weathering of minerals such as the micas biotite and muscovite leading to a release of Mg and K into soil solution, which may have contributed to the large slow-reacting pool of both elements. Weathering of micas is a gradual transformation of their structures by removal of Mg, Fe, and K (Stoch & Sikora, 1976). During biotite weathering in the pH range of 2–6, Mg and Fe are preferentially released (Bray et al., 2015), likely together with K. In the Hailuogou region, the Mg release was closely correlated with that of Fe and Al, but not with the CO_3^{2-} concentrations indicating that most of the released Mg was associated with silicate weathering.

Contrary to our hypothesis, the fast-reacting Pool A of Mg did not significantly change with time and was consistently smaller than the slow-reacting Pool B of Mg along the chronosequence (Figure 5b). The size of Pool A of Mg correlated with the exchangeable Mg concentration in soil (Table 2). Only in the younger soils (Sites 1 and 2), Pool A was significantly larger than the exchangeable Mg pool, which we attribute to a slightly higher chlorite concentration at Sites 1 and 2 (4%, Zhou et al., 2016), because chlorite is easily weatherable and can be quickly lost from the topsoil (Terhorst et al., 2012). The finding that 2 h after the start, before the slow-reacting pool of Mg was activated, the molar K/Mg ratio significantly decreased with site age from 3.4 ± 0.2 (Site 1) to 1.2 ± 0.3 (Site 7) (Figure 7a), while after 168 h the K/Mg ratios did not correlate with site age anymore indicated that more Mg was leached relative to K, although more K than Mg was originally stored in the mineral soil (K/Mg ratio in the mineral soil: 1.3 ± 0.1, Figure 7b). This was in line with the findings of Basdediós et al. (2022), who reported a decrease in the total stocks of Mg along the chronosequence, while those of K were not related to ecosystem age.

We suggest that Ca was initially mainly released from calcite, while Mg was released from chlorite. At later stages of the chronosequence, bioavailable (fast-reacting) Ca and Mg were stored in the exchangeable pools, which was replenished by the slow weathering of silicate minerals of intermediate stability such as titanite for Ca and hornblende and biotite for Mg. After 127 yr, the contributions of hornblende and biotite to the total mineral mass had decreased from 11.8 to 8.5% and from 18.0 to 9.0% (Zhou et al., 2016), respectively, from which we infer that these two minerals contributed to the slow-reacting Pool B of Mg (Figure 5b).

4.4 | Source minerals of K and Na release

The release of K was one order of magnitude higher than that of Na (Figure 4c,d), although the total concentrations of both elements were similar in the parent material (Table 1). In line with the findings of Basdediós et al. (2022), the size of the Pools A and B of both elements did not correlate with site age, although the slow-reacting Pool B of K showed a marginally significant ($p < .1$) decreasing trend that may become more pronounced in the longer term (e.g., Lichter, 1998).

The finding that the fast-reacting Pools A of K and Na were consistently larger than their respective exchangeable pools (Figure 6c,d), indicated the presence of reactive K and Na pools in the soil that were not salt extractable. A possible source of this reactive K might be the interlayers of clay minerals, which can contain substantial, not salt-extractable K concentrations but can be easily weathered (Falk Øgaard & Krogstad, 2005). Extensive depletion of interlayer K in clay minerals might also have contributed to the decrease in the K release rate constants of the slow-reacting K pool (k_{b_K}) with age (Table 2), because the release of interlayer K usually decreases when the concentration of K in soil solution increases (Hinsinger & Jaillard, 1993). The small fast-reacting pool of Na might be related to the presence of low concentration of Na carbonates in the glacial debris (Zhou et al., 2016).

With increasing site age, the K release from the slow-reacting K pool decreased (Table 2) indicating that less primary K was delivered into the soil solution. We attribute the large slow-reacting K pool to the weathering of minerals such as biotite, which also released Mg (Figure 5b,c) and muscovite. The slow-reacting Na pool was also consistently larger than the fast-reacting Na pool and increased marginally significantly with increasing Na concentrations in the soil indicating that most of the Na present in the study soils was associated with weathering-resistant minerals, such as Na-rich feldspar and augite. Interestingly, the significantly largest Pool B of Na at the 57-yr site (Figure 5d) was consistent with the report of Zhou et al. (2016) that at this site the augite concentration in topsoil was with 5.9% the highest along the chronosequence. The other soils only contained 2.1–3.1% of augite. This supports our assumption that augite contributed to the slow-reacting Pool B of Na. Moreover, in granitic substrates, plagioclases (Ca and Na feldspars) are usually faster weathered than K-feldspars (Grant, 1962), while the Ca-rich end member of the plagioclases dissolves faster than the Na-rich end-member (Palandri & Kharaka, 2004), contributing to the more rapid release of Ca than Na along the chronosequence (Figure 4). The faster release of Ca might also explain why stream water samples in the Hailuogou region were dominated by Ca, while Na only accounted for a small proportion of the dissolved base cations (Zhou et al., 2016). Therefore, we infer that the weathering of Na-containing minerals along the Hailuogou chronosequence released much less Na than other base cations (Figure 4). As a consequence, the Na stocks remained almost constant along the chronosequence (Basdediós et al., 2022).

5 | CONCLUSIONS

Although the Gongga peak is mainly composed of granite and granitoid rocks, sedimentary rocks in the eastern catchment area of the Hailuogou glacier contribute $CaCO_3$ to the Hailuogou glacial debris, from which the studied chronosequence developed. Calcite was mainly present in the pores of the metasedimentary rocks as interstitial calcite in the silicate matrix. We have detected carbonates even in the granitoid rocks, which we attribute to a combination of magmatic processes with external inputs during rock formation.

The fast initial weathering of carbonates determined the rapid initial Ca release. The Mg release was, in contrast, closely correlated with Fe and Al release, but not with the carbonate concentrations, indicating that most of the released Mg was associated with silicate weathering. The sizes of the fast-reacting pools of Ca and Mg mostly matched the sizes of their respective exchangeable pools. The slow-reacting pool of Mg was considerably larger than the fast-reacting pool of Mg, which indicated that Mg was generally stored in more stable minerals than Ca, such as in biotite and hornblende.

The main sources of weathered K and Na were silicate minerals. The release of K was one order of magnitude higher than that of Na, although the total concentration of both elements were similar in the parent material. With increasing site age, the K release from the slow-reacting K pool slowed down so that increasingly less primary K was delivered into the soil solution. The weathering of Na-containing minerals along the Hailuogou chronosequence released little Na so that the Na stocks remained nearly constant during the 127-yr succession.

Our results suggest that the fast weathering of carbonates in the otherwise acidic, granite-dominated glacial till allowed for a fast initial delivery of Ca, succeeded by an increasing weathering of silicates with decreasing pH and a subsequent delivery of other nutrients including K and Mg could have facilitated the fast vegetation succession. The slower base cation release after the carbonates had been completely leached, fell together with a change of the forest composition from deciduous to coniferous with a lower nutrient demand. Thus, the vegetation development seemed to be synchronized with the weathering regime.

ACKNOWLEDGMENTS

We thank Z. Zhong, J. Wang, H. Bing, J. Zhou, and Q. He, as well as many students from the Chinese Academy of Science for their support in the field during the sampling campaign, Stephan Unrein for providing the thin sections, and Armin Zeh for his help in classifying the rocks, taking the photomicrographs and evaluating the mineral composition. We are indebted to the German Research Foundation (DFG, Wi 1601/25-1) and to the National Natural Science Foundation of China (42271064) for funding this study.

AUTHOR CONTRIBUTIONS

Nuria Basdediós: Data curation; Formal analysis; Investigation; Methodology; Project administration; Validation; Visualization; Writing – original draft. Yanhong Wu: Conceptualization; Funding acquisition; Investigation; Project administration; Resources; Supervision; Writing – review & editing. Wolfgang Wilcke: Conceptualization; Funding acquisition; Investigation; Methodology; Project administration; Resources; Supervision; Writing – review & editing.

CONFLICT OF INTEREST

The authors declare no conflict of interest.

ORCID

Wolfgang Wilcke https://orcid.org/0000-0002-6031-4613

REFERENCES

Allen, B. L., & Hajek, B. F. (1989). Mineral occurrence in soil environments. In J. B. Dixon & S. B. Weed (Eds.), *Soils in mineral environments* (2nd ed., pp. 199–278). SSSA. https://doi.org/10.2136/sssabookser1.2ed.c5

Alt, F., Oelmann, Y., Schoning, I., & Wilcke, W. (2013). Phosphate release kinetics in calcareous grassland and forest soils in response to H^+ addition. *Soil Science Society of America Journal*, *77*, 2060–2070. https://doi.org/10.2136/sssaj2013.02.0072

Anderson, D. W. (1988). The effect of parent material and soil development on nutrient cycling in temperate ecosystems. *Biogeochemistry*, *5*, 71–97. https://doi.org/10.1007/BF02180318

Andersson, S., & Nilsson, S. I. (2001). Influence of pH and temperature on microbial activity, substrate availability of soil-solution bacteria and leaching of dissolved organic carbon in a mor humus. *Soil Biology & Biochemistry*, *33*, 1181–1191. https://doi.org/10.1016/S0038-0717(01)00022-0

Augusto, L., Achat, D. L., Jonard, M., Vidal, D., & Ringeval, B. (2017). Soil parent material—A major driver of plant nutrient limitations in terrestrial ecosystems. *Global Change Biology*, *23*, 3808– 3824. https://doi.org/10.1111/gcb.13691

Barker, W. W., Welch, S. A., & Banfield, J. F. (1997). Biogeochemical weathering of silicate minerals. In J. F. Banfield, & K. H. Nealson (Eds.), *Geomicrobiology: Interactions between microbes and minerals* (Reviews in Mineralogy, vol. 35, pp. 391–428). Mineralogical Society of America.

Basdediós, N., Zhong, Z., Wu, Y., & Wilcke, W. (2022). Initial carbonate weathering is linked with vegetation development along a 127-year glacial retreat chronosequence in the subtropical high mountainous Hailuogou region (SW China). *Plant and Soil*, *471*, 609–628. https://doi.org/10.1007/s11104-021-05250-y

Berner, E. K., Berner, R. A., & Moulton, K. L. (2004). Plants and mineral weathering: Past and present. In J. I. Drever (Ed.), *Surface and ground water, weathering, and soils* (Treatise on Geochemistry 5, pp. 169–188). Elsevier. https://doi.org/10.1016/B0-08-043751-6/05175-6

Blum, J. D., Gazis, C. A., Jacobson, A. D., & Chamberlain, C. P. (1998). Carbonate versus silicate weathering in the Raikhot watershed within the high Himalayan crystalline series. *Geology*, *265*, 411– 414. https://doi.org/10.1130/0091-7613(1998)026⟨0411:CVSWIT⟩2.3.CO;2

Bockheim, J. G. (1980). Solution and use of chronofunctions in studying soil development. *Geoderma*, *24*, 71–85. https://doi.org/10.1016/0016-7061(80)90035-X

Bray, A. W., Oelkers, E. H., Bonneville, S., Wolff-Boenisch, D., Potts, N. J., Fones, G., & Benning, L. G. (2015). The effect of pH, grain size, and organic ligands on biotite weathering rates. *Geochimica et Cosmochimica Acta*, *164*, 127–145. https://doi.org/10.1016/j.gca.2015.04.048

Cappuynus, V., & Swennen, R. (2008). The application of pH_{stat} leaching tests to assess the pH-dependent release of trace metals from soils, sediments and waste materials. *Journal of Hazardous Materials*, *158*, 185–195. https://doi.org/10.1016/j.jhazmat.2008.01.058

Chadwick, O. A., & Chorover, J. (2001). The chemistry of pedogenic thresholds. *Geoderma*, *100*, 321–353. https://doi.org/10.1016/S0016-7061(01)00027-1

Deines, P. (1980). The isotopic composition of reduced organic carbon. In P. Fritz, & J. C.h. Fontes (Eds.), *Handbook of environmental isotope geochemistry, Volume 1, The Terrestrial Environment, A* (pp. 329–402). Elsevier Scientific Publishing Company.

Deines, P., & Gold, D. P. (1973). The isotopic composition of carbonatite and kimberlite carbonates and their bearing on the isotopic composition of deep-seated carbon. *Geochimica et Cosmochimica Acta*, *37*, 1709–1733.

Drever, J. I., & Stillings, L. L. (1997). The role of organic acids in mineral weathering. *Colloids and Surfaces A: Physicochemical and Engineering Aspects*, *120*(1–3), 167–181. https://doi.org/10.1016/S0927-7757(96)03720-X

Eimil-Fraga, C., Rodríguez-Soalleiro, R., Sánchez-Rodríguez, F., Pérez-Cruzado, C., & Álvarez-Rodríguez, E. (2014). Significance of bedrock as a site factor determining nutritional status and growth of maritime pine. *Forest Ecology and Management*, *331*, 19–24. https://doi.org/10.1016/j.foreco.2014.07.024

Falk Øgaard, A., & Krogstad, T. (2005). Release of interlayer potassium in Norwegian grassland soils. *Journal of Plant Nutrition and Soil Science*, *168*, 80–88. https://doi.org/10.1002/jpln.200421454

Ghent, E. D., & O'Neil, J. R. (1985). Late Precambrian marbles of unusual carbon-isotope composition, southeastern British Columbia. *Canadian Journal Earth Science*, *22*, 324–329. https://doi.org/10.1139/e85-032

Grant, W. H. (1962). Weathering of Stone Mountain Granite. *Clays and Clay Minerals*, *11*(1), 65–73. https://doi.org/10.1346/ccmn.1962.0110106

Hacker, N., Gleixner, G., Lange, M., Wilcke, W., & Oelmann, Y. (2017). Phosphorus release from mineral soil by acid hydrolysis: Method development, kinetics, and plant community composition effects. *Soil Science Society of America Journal*, *81*, 1389–1400. https://doi.org/10.2136/sssaj2017.02.0064

Harley, A., & Gilkes, R. (2000). Factors influencing the release of plant nutrient elements from silicate rock powders: A geochemical overview. *Nutrient Cycling in Agroecosystems*, *56*, 11–36. https://doi.org/10.1023/A:1009859309453

Hinsinger, P. (2001). Bioavailability of soil inorganic P in the rhizosphere as affected by root-induced chemical changes: A review. *Plant and Soil*, *237*, 173–195. https://doi.org/10.1023/A:1013351617532

Hinsinger, P., & Jaillard, B. (1993). Root-induced release of interlayer potassium and vermiculitization of phlogopite as related to potassium depletion in the rhizosphere of ryegrass. *Journal of Soil Science*, *44*, 525–534. https://doi.org/10.1111/j.1365-2389.1993.tb00474.x

Houlton, B. Z., Morford, S. L., & Dahlgren, R. A. (2018). Convergent evidence for widespread rock nitrogen sources in Earth's surface environment. *Science*, *360*, 58–62. https://doi.org/10.1126/science.aan4399

Huggett, R. J. (1998). Soil chronosequences, soil development, and soil evolution: A critical review. *Catena*, *32*, 155–172. https://doi.org/10.1016/S0341-8162(98)00053-8

IUSS Working Group WRB. (2014). *World Reference Base for soil resources. International soil classification system for naming soils and creating legends for soil maps* (World Soil Resource Reports no. 106). FAO.

Jenny, H. (1941). *Factors of soil formation: A system of quantitative pedology*. McGraw Hill.

Jesse Hahm, W., Riebe, C. S., Lukens, C. E., & Araki, S. (2014). Bedrock composition regulates mountain ecosystems and landscape evolution. *Proceedings of the National Academy of Sciences of the United States of America*, *111*(9), 3338–3343. https://doi.org/10.1073/pnas.1315667111

Jobbágy, E. G., & Jackson, R. B. (2004). The uplift of soil nutrients by plants: Biogeochemical consequences across scales. *Ecology*, *85*, 2380–2389. https://doi.org/10.1890/03-0245

Kaupenjohann, M., & Wilcke, W. (1995). Heavy metal release from a serpentine soil using a pH-stat technique. *Soil Science Society of America Journal*, *59*, 1027–1031. https://doi.org/10.2136/sssaj1995.03615995005900040010x

Li, Z., He, Y., Yang, X., Theakstone, W H., Jia, W., Pu, T., Liu, Q., He, X., Song, B., Zhang, N., Wang, S., & Du, J. (2010). Changes of the Hailuogou glacier, Mt. Gongga, China, against the background of climate change during the Holocene. *Quaternary International*, *218*, 166–175. https://doi.org/10.1016/j.quaint.2008.09.005

Lichter, J. (1998). Rates of weathering and chemical depletion in soils across a chronosequence of Lake Michigan sand dunes. *Geoderma*, *85*, 255–282. https://doi.org/10.1016/S0016-7061(98)00026-3

Lilienfein, J. W. W., Thomas, R., Vilela, L., Lima, S. C., & Zech, W. (2001). Efects of *Pinus caribaea* plantations on the C, N, P, and S status of Brazilian savanna Oxisols. *Forest Ecological Management*, *147*, 171–182. https://doi.org/10.1016/S0378-1127(00)00472-2

Marschner, P. (2012). *Marschner's mineral nutrition of higher plants* (3rd ed.). Academic Press.

Mavris, C., Egli, M., Plötze, M., Blum, J. D., Mirabella, A., Giaccai, D., & Haeberli, W. (2010). Initial stages of weathering and soil formation in the Morteratsch proglacial area. *Geoderma*, *155*, 359–371. https://doi.org/10.1016/j.geoderma.2009.12.019

Meyer, S., De Angeli, A., Fernie, A. R., & Martinoia, E. (2009). Intra- and extra-cellular excretion of carboxylates. *Trends in Plant Science*, *15*, 40–47. https://doi.org/10.1016/j.tplants.2009.10.002

Palandri, J. L., & Kharaka, Y. K. (2004). A compilation of rate parameters of water-mineral interaction kinetics for application to geochemical modeling, in U.S. In Geological survey 2004–1068. U.S. Geological Survey. https://doi.org/10.3133/ofr20041068

Qi, J., Xu, M., An, C., Wu, M., Zhang, Y., Li, X., Zhang, Q., & Lu, G. (2017). Characterizations of geothermal springs along the Moxi deep fault in the western Sichuan plateau, China. *Physics of the Earth and Planetary Interiors*, *263*, 12–22. https://doi.org/10.1016/j.pepi.2017.01.001

R Core Team. (2019). *R: A language and environment for statistical computing*. R Foundation for Statistical Computing. https://www.R-project.org

Roger, F., Calassou, S., Lancelot, J., Malavieille, J., Mattauer, M., Zhiqin, X., Ziwen, H., & Liwei, H. (1995). Miocene emplacement and deformation of the Konga Shan granite (Xianshui He fault, west Sichuan, China): Geodynamic implications. *Earth and Planetary Science Letters*, *130*, 201–216. https://doi.org/10.1016/0012-821X(94)00252-T

Schmitt, A. D., Vigier, N., Lemarchand, D., Millot, R., Stille, P., & Chabaux, F. (2012). Processes controlling the stable isotope compositions of Li, B, Mg and Ca in plants, soils and waters: A review. *Comptes Rendus - Geoscience*, *344*, 704–722. https://doi.org/10.1016/j.crte.2012.10.002

Schwarcz, H. P. (1969). Carbon. In K. H. Wedepohl (Ed.), *Handbook of geochemistry*. *Section B-I. The stable isotopes of carbon* (pp. 6–B–1–6–B–15). Springer-Verlag.

Schwarz, A., Wilcke, W., Styk, J., & Zech, W. (1999). Heavy metal release from soils in batch pH(stat) experiments. *Soil Science Society of America Journal*, *63*, 290–296. https://doi.org/10.2136/sssaj1999.03615995006300020006x

Searle, M. P., Roberts, N. M. W., Chung, S. L., Lee, Y.-H., Cook, K. L., Elliott, J. R., Weller, O. M., St-Onge, M. R., Xu, Xi-W., Tan, Xi-B., & Li, K. (2016). Age and anatomy of the Gongga Shan batholith, eastern Tibetan Plateau, and its relationship to the active Xianshui-he fault. *Geosphere*, *12*, 948–970. https://doi.org/10.1130/GES01244.1

Selim, H. M., & Amacher, M. C. (1997). *Reactivity and transport of heavy metals in soils*. CRC Press.

Smith, K. S., & Huyck, H. L. O. (1999). An overview of the abundance, relative mobility, bioavailability, and human toxicity of metals. In G. S. Plumlee & M. J. Logsdon (Eds.), *The environmental chemistry of mineral deposits, reviews in economic geology* (Volume 6A, pp. 29–70). Society of Economic Geologists.

Sohrt, J., Lang, F., & Weiler, M. (2017). Quantifying components of the phosphorus cycle in temperate forests. *WIREs Water*, *4*(6), e1243. https://doi.org/10.1002/wat2.1243

Stoch, L., & Sikora, W. (1976). Transformations of micas in the process of kaolinitization of granites and gneisses. *Clays and Clay Minerals*, *24*, 156–162. https://doi.org/10.1346/CCMN.1976.0240402

Süsser, P. (1987). *Art, Menge und Wirkungsweise von Puffersubstanzen in Mineralbodenhorizonten forstlich genutzter Böden des Fichtelgebirges* [PhD dissertation at the Chair of Soil Science, Technical University Munich, TUM].

Terhorst, B., Ottner, F., & Wriessnig, K. (2012). Weathering intensity and pedostratigraphy of the Middle to Upper Pleistocene loess/palaeosol sequence of Wels-Aschet (Upper Austria). *Quaternary International*, *265*, 142–154. https://doi.org/10.1016/j.quaint.2011.08.042

Tripler, C. E., Kaushal, S. S., Likens, G. E., & Walter, M. T. (2006). Patterns in potassium dynamics in forest ecosystems. *Ecology Letters*, *9*(4), 451–466. https://doi.org/10.1111/j.1461-0248.2006.00891.x

van de Sand, M., & Fischer, W. R. (1994). Quantifizierung der wichtigsten Mechanismen zur Säurepufferung carbonatfreier Böden. *Zeitschrift Für Pflanzenernährung und Bodenkunde*, *157*, 369–373.

Vitousek, P. M., & Sanford, R. L. (1986). Nutrient cycling in moist tropical forest. *Annual Review of Ecology and Systematics*, *17*, 137–167. https://doi.org/10.1146/annurev.es.17.110186.001033

Walker, L. R., Wardle, D. A., Bardgett, R. D., & Clarkson, B. D. (2010). The use of chronosequences in studies of ecological succession and soil development. *Journal of Ecology*, *98*, 725–736. https://doi.org/10.1111/j.1365-2745.2010.01664.x

White, P. J., & Broadley, M. R. (2003). Calcium in plants. *Annals of Botany*, *92*(4), 487–511. https://doi.org/10.1093/aob/mcg164

White, A. F., Bullen, T. D., Vivit, D. V., , Schulz, M. S., & Clow, D. W. (1999). The role of disseminated calcite in the chemical weathering of granitoid rocks. *Geochimica et Cosmochimica Acta*, *63*, 1939–1953. https://doi.org/10.1016/S0016-7037(99)00082-4

White, A. F., Schulz, M. S., Lowenstern, J. B., Vivit, D V., & Bullen, T D. (2005). The ubiquitous nature of accessory calcite in granitoid rocks: Implications for weathering, solute evolution, and petrogenesis. *Geochimica et Cosmochimica Acta*, *69*, 1455–1471. https://doi.org/10.1016/j.gca.2004.09.012

Wilcke, W., Yasin, S., Abramowski, U., Valarezo, C., & Zech, W. (2002). Nutrient storage and turnover in organic layers under tropical montane rain forest in Ecuador. *European Journal of Soil Science*, *53*, 15–27. https://doi.org/10.1046/j.1365-2389.2002.00411.x

Wilson, M. (2004). Weathering of the primary rock-forming minerals: Processes, products and rates. *Clay Minerals*, *39*(3), 233–266. https://doi.org/10.1180/0009855043930133

Wu, Y., Li, W., Zhou, J., & Cao, Y. (2013). Temperature and precipitation variations at two meteorological stations on eastern slope of Gongga Mountain, SW China in the past two decades. *Journal of Mountain Science*, *10*, 370–377. https://doi.org/10.1007/s11629-013-2328-y

Yang, Z., Bing, H., Zhou, J., Wu, Y., Sun, H., Luo, J., Sun, S., & Wang, J. (2015). Variation of mineral composition along the soil chronosequence at the Hailuogou glacier foreland of Gongga Mountain. *Acta Pedologica Sinica*, *52*, 39–48. https://doi.org/10.11766/trxb201406180301

Zamanian, K., Pustovoytov, K., & Kuzyakov, Y. (2016). Pedogenic carbonates: Forms and formation processes. *Earth-Science Reviews*, *157*, 1–17. https://doi.org/10.1016/j.earscirev.2016.03.003

Zhou, J., Bing, H., Wu, Y., Yang, Z., Wang, J., Sun, H., Luo, J., & Liang, J. (2016). Rapid weathering processes of a 120-year-old chronosequence in the Hailuogou Glacier foreland, Mt. Gongga, SW China. *Geoderma*, *267*, 78–91. https://doi.org/10.1016/j.geoderma.2015.12.024

Zhou, J., Wu, Y., Prietzel, J., Bing, H., Yu, D., Sun, S., Luo, J., & Sun, H. (2013). Changes of soil phosphorus speciation along a 120-year soil chronosequence in the Hailuogou Glacier retreat area (Gongga Mountain, SW China). *Geoderma*, *195–196*, 251–259. https://doi.org/10.1016/j.geoderma.2012.12.010

How to cite this article: Basdediós, N., Wu, Y., & Wilcke, W. (2022). Base cations release in soils along the 127-year Hailuogou glacial retreat chronosequence. *Soil Science Society of America Journal*, *86,* 1692–1706. https://doi.org/10.1002/saj2.20473